Published Ahead of Print on March 24, 2016 as 10.5966/sctm.2015-0233.

STEM CELLS TRANSLATIONAL MEDICINE®

TISSUE ENGINEERING AND REGENERATIVE MEDICINE

Chondroitin Sulfate Immobilized on a Biomimetic Scaffold Modulates Inflammation While Driving Chondrogenesis

BRUNA CORRADETTI,[a,b,*] FRANCESCA TARABALLI,[a,*] SILVIA MINARDI,[a,c] JEFFREY VAN EPS,[a,d] FERNANDO CABRERA,[a] LEWIS W. FRANCIS,[e] SALVATORE A. GAZZE,[e] MAURO FERRARI,[a,f] BRADLEY K. WEINER,[a,g] ENNIO TASCIOTTI[a]

Key Words. Mesenchymal stem cells • Chondroitin sulfate • Chondrogenic differentiation • Immunosuppression • Tissue engineering • Biomimetic scaffolds • Arthritis

ABSTRACT

Costs associated with degenerative inflammatory conditions of articular cartilage are exponentially increasing in the aging population, and evidence shows a strong clinical need for innovative therapies. Stem cell-based therapies represent a promising strategy for the treatment of innumerable diseases. Their regenerative potential is undeniable, and it has been widely exploited in many tissue-engineering approaches, especially for bone and cartilage repair. Their immune-modulatory capacities in particular make stem cell-based therapeutics an attractive option for treating inflammatory diseases. However, because of their great plasticity, mesenchymal stem cells (MSCs) are susceptible to different external factors. Biomaterials capable of concurrently providing physical support to cells while acting as synthetic extracellular matrix have been established as a valuable strategy in cartilage repair. Here we propose a chondroitin sulfate-based biomimetic scaffold that recapitulates the physicochemical features of the chondrogenic niche and retains MSC immunosuppressive potential in vitro, either in response to a proinflammatory cytokine or in the presence of stimulated peripheral blood mononuclear cells. In both cases, a significant increase in the production of molecules associated with immunosuppression (nitric oxide and prostaglandins), as well as in the expression of their inducible enzymes (*iNos*, *Pges*, *Cox-2*, and *Tgf-β*). When implanted subcutaneously in rats, our scaffold revealed a reduced infiltration of leukocytes at 24 hours, which correlated with a greater upregulation of genes involved in inflammatory cell apoptotic processes. In support of its effective use in tissue-engineering applications of cartilage repair, the potential of the proposed platform to drive chondrogenic and osteogenic differentiation of MSC was also proven. STEM CELLS TRANSLATIONAL MEDICINE *2016;5:1–13*

SIGNIFICANCE

Recently, increasing clinical evidence has highlighted the important role of proinflammatory mediators and infiltrating inflammatory cell populations inducing chronic inflammation and diseases in damaged cartilage. This work should be of broad interest because it proposes an implantable biomimetic material, which holds the promise for a variety of medical conditions that necessitate the functional restoration of damaged cartilage tissue (such as trauma, diseases, deformities, or cancer).

INTRODUCTION

Articular cartilage damage is an increasingly relevant problem, further enhanced with the aging population. In the U.S., 70 million adults have arthritis-related conditions; this leads to increasing annual costs, which are estimated to reach $100 billion by 2020 [1, 2]. Restorative treatments to achieve biological repair remain a challenge [3]. Surgical intervention is reserved for patients with severe degenerative diseases and those in whom pharmacologic and lifestyle interventions fail; such patients usually require total joint replacement with articular prosthesis [4–7]. The idea of artificial cartilage has become greatly attractive because of the lack of grafts and the high demand for such a product in clinical practice [8]. Regenerative medicine could point the way toward an innovative solution. A foundational principle of regenerative medicine is creating an environment where progenitor cells are able to develop functional tissue in order to replace those lost because of traumas or diseases [9]. Many regenerative medicine strategies use biomaterials to provide mechanical stability and support cell adhesion and migration [10]. Aside from these properties, a regenerative biomaterial should also fulfill

[a]Department of Nanomedicine, Houston Methodist Research Institute, Houston, Texas, USA; [b]Department of Life and Environmental Sciences, Polytechnic University of Marche, Ancona, Italy; [c]Institute of Science and Technology for Ceramics, National Research Council of Italy, Faenza, Italy; Departments of [d]Surgery and [g]Orthopedics & Sports Medicine, Houston Methodist Hospital, Houston, Texas, USA; [e]Centre for NanoHealth, Swansea University Medical School, Swansea University Bay, Singleton Park, Wales, United Kingdom; [f]Department of Medicine, Weill Cornell Medical College, New York, New York, USA

[*]Contributed equally.

Correspondence: Ennio Tasciotti, Ph.D., Department of Nanomedicine, Houston Methodist Research Institute, 6670 Bertner Avenue, Houston, Texas 77030, USA. Telephone: 713-441-7319; E-Mail: ETasciotti@houstonmethodist.org.

Received September 10, 2015; accepted for publication January 4, 2016.

1066-5099/2016/$20.00/0

http://dx.doi.org/10.5966/sctm.2015-0233

Published Ahead of Print on March 24, 2016 as 10.5966/sctm.2015-0233.

multiple other requirements, including modulation of the initial inflammatory response to injury. The immune reaction to a biomaterial implant begins with an acute inflammatory response with innate recognition of foreign materials, which can eventually lead to the rejection of the implant [11] or induce additional tissue damage [12]. In both cases, chronic inflammation impedes the natural repair processes led by local progenitor and mature cells.

The development of strategies that harness the beneficial aspects of the immune response while limiting their potential deleterious effects enhances tissue regeneration, especially in those tissues, such as cartilage, in which the process of regeneration remains challenging [13]. In particular, when cartilage is damaged, its avascularity prevents the cascade that occurs in normal tissue and the dense extracellular matrix (ECM) impairs the migration capacity of the resident chondrocytes [14–16]. These are the two major limitations to the cartilage regeneration. Within cartilage ECM, collagen is the most abundant protein component [17], and it has been used as a natural biomaterial for different tissue-engineering applications [6, 18–24].

The other major component of cartilage is represented mainly by aggrecan, a large proteoglycan composed of many glycosaminoglycans [25]. Among these, chondroitin sulfate (CS) is one of the most represented [26]. Proteoglycans play a crucial role in intercellular communications that regulate important physiological processes, including growth factor retention, cellular adhesion/proliferation support, differentiation induction, and provision of mechanical properties [27, 28]. Because of its intrinsic stability and low immunogenicity in comparison with most ECM proteins, aggrecan (specifically CS) plays an important role in inflammation and immunity [29–36]. Both in vitro and in vivo studies have shown that CS itself regulates the formation of new cartilage by stimulating the chondrocyte synthesis of collagen, proteoglycans, and hyaluronan [37, 38].

Altogether, these features make CS a material of choice for cartilage tissue engineering [28, 39]. To date, CS has been immobilized onto different surfaces to exploit its role in recreating the chondrogenic niche in vitro, and potentially in vivo [40–42]. Despite the advancements in material development, the immunosuppressive potential of this biomimetic material have not been investigated in depth. Understanding the capability of a biomaterial to support adhesion, proliferation, and differentiation of progenitor cells is crucial to restore functional tissue.

This applies particularly to mesenchymal stem cells (MSCs), which contribute to tissue homeostasis via release of bioactive molecules at sites of tissue damage. MSC secrete trophic factors that act as anti-inflammatory immune modulators [43, 44], thus enhancing tissue repair [45]. MSCs exhibit multipotent capability [46] and have been extensively investigated in regenerative medicine applications [47–49], as well as in combination with scaffolds [50]. Despite extensive research on cartilage tissue engineering, few products have been translated to clinical practice, and an effective engineered clinical therapy is lacking [18].

In this study, we propose a collagen-based scaffold functionalized with CS to mimic the chondrogenic niche while modulating inflammation. In addition to describing the proposed material in terms of composition, swelling, degradation, and mechanical properties, we evaluated the effect of our biomaterial to support the capability of MSCs to exert therapeutic effects, with particular emphasis on their potential to actively respond to an inflammatory environment [51]. Using rat bone marrow-derived MSCs as surrogate local progenitor cells, we investigated the influence of a chondrogenic environment in retaining the immunosuppressive potential of MSCs, either in response to a proinflammatory cytokine (tumor necrosis factor-α [TNF-α]) or in the presence of stimulated peripheral blood mononuclear cells (PBMCs).

We confirmed the capability of CS crosslinked onto a collagen-based scaffold (CSCL) to reduce inflammation in vivo by evaluating lymphocytic infiltration upon subcutaneous implantation in rodents. We also assessed the potential of the proposed platform to drive chondrogenic and osteogenic differentiation of MSCs.

Materials and Methods

Scaffold Preparation

Collagen scaffolds were fabricated with the freeze-dry technique previously reported. Briefly, we prepared an acetic collagen slurry (40 mg/ml), which was precipitated to a pH of 5.5 with NaOH (1.67 mM). The slurry was wet crosslinked in an aqueous solution of 1,4-butanediol diglycidyl ether (2.5 mM) at 4°C for 24 hours. Finally, the slurry was washed with Milli-Q water scaffolds (EMD Millipore, Darmstadt, Germany, http://www.emdmillipore.com) and prepared through a freeze-drying process. Chondroitin sulfate (Carbosynth, Berkshire, U.K., http://www.carbosynth.com/) was added to the collagen solution at a weight molar ratio of 10:1 (CL:CS). After thorough mixing, the final slurry was poured onto a 24-well plate and freeze-dried. CSCL was crosslinked for 4 hours at 37°C by using 50 mM 2-(*N*-morpholino)ethanesulfonic acid, 5 mM 1-ethyl-3-(3-dimethylaminopropyl)carbodiimide (EDC), and 5 mM *N*-hydroxysuccinimide. CSCL scaffolds were then rinsed twice for 1 hour with 0.1 M disodium phosphate and 6 times for 24 hours with 2 M sodium chloride; finally, they were rinsed with distilled water to remove residual EDC. Scaffolds were air-dried and sterilized by ultraviolet irradiation for 4 hours under a laminar flow hood.

Scaffold Characterization

Scaffolds were dehydrated by treatment with a grade of ethanol solutions (30%, 50%, 75%, 85%, and 95% for 2 hours each) and placed overnight in a dryer at room temperature before being coated by 7 nm of Pt/Pl for scanning electron microscope (SEM; Nova NanoSEM 230, FEI, Hillsboro, OR, http://www.fei.com) examination. The pore diameter of scaffolds was measured from SEM images, and 6 images were used for each scaffold at the same magnitude. For each image, 20 different pores were randomly selected and their diameters were measured by using ImageJ software (National Institutes of Health, Bethesda, MD, http://imagej.nih.gov/ij). To determine the porosity (P) of the scaffolds, we used a capillary method previously reported [52]. The volumes of the scaffolds (*Vs*) were calculated from the scaffold geometry (length, width, and height). The volume of pores (*Vp*) was calculated by an ethanol infiltration method using Equation 1:

$$V_p = (We - W0)/\rho e \quad (1)$$

where *We* is the weight of the scaffold after ethanol incubation, *W0* is the weight of the dry scaffold, and ρe is the density of the ethanol (0.789 mg·ml^{-1}). The porosity of the scaffolds was calculated according to $P = Vp/Vs$ 100%. The apparent density of the scaffolds was defined as *W0/Vs*.

Mechanical Characterization

The elastic properties of the scaffolds were evaluated with atomic force microscopy (AFM) by extracting the Young's modulus from

Published Ahead of Print on March 24, 2016 as 10.5966/sctm.2015-0233.

AFM-acquired force curves: a BioScope Catalyst AFM (Bruker Instruments, Santa Barbara, CA, https://www.bruker.com) was used, in tandem with MLCT-E silicon nitride cantilevers (Bruker Instruments), with spring constant and deflection sensitivity experimentally determined before each measurement. For each scaffold type, 18 different 4-μm^2 areas were considered, with 100 equally spaced force curves obtained on each area. The contact regimen of the approach part of each force curve was fitted with the equation of a spherical indenter (Hertz model, Equation 2) by using the fitting module of Nanoscope Analysis software, v1.50 (Bruker AFM Probes, Camarillo, CA, http://www.brukerafmprobes.com), and the elastic module (Young's module) in each force curve was extracted according to Equation 2:

$$F = \frac{4E\sqrt{R}\,\delta^{3/2}}{3\,(1-\upsilon^2)} \quad (2)$$

In Equation 2, F is the force applied by the cantilever tip to the scaffold (5 nN), E is the Young's modulus (fit parameter), υ is the Poisson ratio (0.5), and R is the radius of the indenter (i.e., of the cantilever tip; 20 nm). Only force curves with a goodness of fit to Equation 2 between 0.85 and 1 were considered. Data distribution and statistical analysis were performed using Mathematica 9.0 (Wolfram, Champaign, IL, https://www.wolfram.com) and Minitab, v.14.1 (Minitab Inc., State College, PA, https://www.minitab.com) [53]. Normality was evaluated by using the Anderson-Darling (AD) test, with $p \leq .005$ used as a threshold for significance.

Fourier Transform Infrared Spectroscopy

The samples were analyzed in attenuated total reflection (ATR) mode at 2 cm^{-1} resolution 256 times over the range of 500–4,000 cm^{-1} using a Nicolet 6700 spectrometer (ThermoFisher Scientific, Waltham, MA, http://www.thermofisher.com). The ATR/Fourier transform infrared spectroscopy (FTIR) spectra were reported after background subtraction, baseline correction, and binomial smoothing (11 points) [54].

Thermal Gravimetric Analysis and Differential Scanning Calorimetry

Thermal gravimetric analysis (TGA) and differential scanning calorimetry (DSC) were performed using a TGA/DSC simultaneous thermogravimetric analyzer (Q600, TA Instruments, New Castle, DE, http://www.tainstruments.com). Ten milligrams of each sample were placed in alumina pans and analyzed through a heating ramp ranging from 25°C and 400°C at 10°C/minute. Data were analyzed through the TA Universal Analysis software (TA Instruments).

Degradation Studies

Three scaffolds for each time point (2, 7, and 21 days) were incubated in 10 ml phosphate-buffered saline (PBS) with or without 10 mg/l hen egg white lysozyme (46,400 U/mg). The enzymatic solution was replaced weekly by freshly prepared solutions. Samples were dehydrated by using a graded series of alcohol, dried in vacuum for 8 hours before weight determination.

Swelling Measurements

To determine the swelling property of CL and CSCL, five completely dried scaffolds were weighted (Wd) and afterward incubated in PBS at 37°C. The hydrated scaffolds were taken out at the determined time points, wiped superficially with a filter paper to remove the surface water, and weighed (Ww). The uptake ratio was defined as percentage swelling, as in Equation 3.

$$\mathrm{Sw}\% = (W\mathrm{w} - W\mathrm{d})/W\mathrm{d} \times 100 \quad (3)$$

Cell Culture

MSCs were isolated from rat bone marrow as previously reported for mice [55]. Cultures were established in standard media constituted by high glucose-Dulbecco's modified Eagle medium (HG-DMEM) supplemented with 15% fetal bovine serum, 1% penicillin (100 UI/ml)-streptomycin (100 mg/ml), and 0.25 mg/ml amphotericin B. For maintenance of cultures, cells were plated at a cell density of 7×10^3 cells per cm^2 and incubated at 37°C in a humidified atmosphere (90%) with 5% CO_2. Medium was changed twice per week thereafter or according to the experiment requirements. Adherent cells were detached and subcultured using TrypLE Express (Invitrogen, ThermoFisher Scientific) before reaching confluence (80%) and subsequently replated for culture maintenance. When seeded onto scaffolds, MSCs were harvested and resuspended in cell culture medium. A 30-μl drop of medium containing 300,000 cells was seeded on the center of each scaffold (CL and CSCL) and kept in an incubator for 30 minutes. Culture medium was then added to each well.

Assessment of MSC Attachment, Spreading, and Viability

Three days after seeding, cells were stained using fluorescent DRAQ5 and captured on a confocal laser microscope (A1 Confocal Microscope, Nikon Instruments, Melville, NY, https://www.nikoninstruments.com) to evaluate their spreading on the scaffolds. Cell spreading on CL and CSCL was calculated on the basis of the auto fluorescence of the collagen detected at 358/461 nm. The surface area covered by cells on the scaffolds was measured and compared with the control, represented by collagen-based scaffolds (NIS-Element, Nikon Instruments). The number of cells per surface area of the collagen-based scaffolds was calculated through an automated counting tool of the software. To evaluate the effect of the CS on cell organization and distribution, the mean distance between cell nuclei was also measured.

Cell proliferation in the scaffolds was evaluated by Alamar Blue assay (Invitrogen, ThermoFisher Scientific) according to manufacturer's instructions during a 6-day period. Optical density was measured at wavelengths of 570 and 600 nm. Because the culture medium was not changed during this period, the calculated percentage of Alamar blue reduction (%AB) is a cumulative value. Data are shown as mean of 3 independent biological replicates. Values are reported as %AB over time, which is associated with the presence of metabolically active cells. For comparison, data obtained from MSCs grown in two-dimensional conditions (2D MSCs) are also reported. To confirm cell viability and visualize viable cells within the scaffold, MSCs were stained using a fluorescent Live-Dead Viability Assay (Molecular Probes, ThermoFisher Scientific, Eugene, OR) according to the manufacturer's instructions on day 3.

Immunosuppressive Potential of MSCs

To evaluate the efficacy of the platform in helping MSCs retain their immunosuppressive potential, cells were seeded onto CL

Published Ahead of Print on March 24, 2016 as 10.5966/sctm.2015-0233.

and CSCL scaffolds and cultured for 24 hours at 37°C before biomolecule stimulation. Stimulation was performed using rat recombinant TNF-α (PeproTech, Rocky Hill, NJ, https://www.peprotech.com) at a concentration of 10 and 50 ng/ml for 48 hours, as previously reported [56]. Cells cultured in 2D conditions, whether stimulated or not, were used as reference. At 48 hours, the activated supernatant and the cells were harvested from the cultures, filtered, and stored at −80°C. After stimulation, the prostaglandin level was measured in cell culture supernatants using a prostaglandin E_2 (PGE_2) enzyme immunoassay kit (Cayman Chemical Co., Ann Arbor, MI, https://www.caymanchem.com) according to the manufacturer's protocol. The presence of nitric oxide (NO) in the culture supernatants was measured by using a nitric oxide (total) detection kit (Enzo Life Sciences, Farmingdale, NY, http://www.enzolifesciences.com) following the manufacturer's instructions. The levels of PGE_2 and NO released from stimulated MSCs seeded onto CL and CSCL were compared with those produced by unstimulated cells grown onto CL or CSCL, respectively.

Testing Proliferation of Peripheral Blood Mononuclear Cells

Rat PBMCs were obtained from heparinized whole-blood samples by using density gradient centrifugation (Lymphoprep, Axis-Shield, Oslo, Norway, http://www.axis-shield-density-gradient-media.com/) following the manufacturer's instructions. PBMC proliferation was induced by stimulating cells with 2% phytohemagglutinin (PHA; Sigma-Aldrich, St. Louis, MO, http://www.sigmaaldrich.com) in a final HG-DMEM complete media. The effect of MSCs grown onto scaffolds (CL or CSCL) on T lymphocyte proliferation was determined in a cell-cell contact setting with MSCs and PBMCs plated at a 1:10 ratio. Twenty-four hours after seeding the MSCs onto CL and CSCL, PBMCs were stained with BD Horizon Violet Cell Proliferation Dye 450 (VPD450; BD Biosciences, San Jose, CA, http://www.bdbiosciences.com) for 10 minutes, washed in PBS, and cocultured. PBMC proliferation was assessed by flow cytometry after 3 days of culture.

In Vivo Studies

Adult Lewis rats (n = 3; Charles River Laboratories, Houston, TX, http://www.criver.com/) were used for in vivo validation studies. All animals were maintained and used in conformity with the guidelines established by American Association for Laboratory Animal Science, and all procedures were approved by the Houston Methodist Institutional Animal Care and Use Committee. Rats received appropriate preoperative analgesia with weight-based subcutaneously injected buprenorphine and carprofen. Induction and maintenance anesthesia was provided using inhaled isoflurane gas, and the dorsum of each animal was shaved from shoulder to hock. Under sterile technique, three skin incisions were made on both sides of the dorsal midline of each animal and the premuscular, avascular subcutaneous plane was developed by using blunt dissection. Into each subcutaneous pocket was placed a 1-cm diameter, 0.3-cm thick scaffold (left side, CL; right side, CS), and all incisions were closed with wound clips. Postoperatively, rats were housed in individual cages, given food and water ad libitum, and kept on a 12-hour light/dark schedule in typical fashion. Twenty-four hours after implantation, animals were humanely euthanized and scaffold specimens were harvested and kept for further analyses.

Histological and Immunohistochemical Analysis

After euthanasia, the implants with surrounding tissue were removed, immersed in 10% buffered formalin phosphate solution for 48 hours, and then embedded in paraffin. Sections were then dewaxed in an incubator for 30 minutes at 60°C before the histological and immunohistochemical stainings were performed. For both assays, 10-μm-thick sections were deparaffinized twice in fresh xylene for 15 minutes and rehydrated sequentially with decreasing ethanol concentrations (100%, 95%, 90%, 80%, and 70%) and distilled water (15 minutes for each step). For histology, Masson's trichrome staining (Abcam, Cambridge, U.K., http://www.abcam.com) was used. For the immunohistochemistry, slides were pretreated using a standard cycle of pressure cooker to unmask epitopes in antigen retrieval solution (0.1 M sodium citrate, pH 7.2). Pretreated slides were blocked for 1 hour at room temperature with 10% normal goat serum and then incubated at 4°C overnight with anti-CD3 antibody (ab5690 abcam). Slides were then washed three times in PBS and finally mounted with ProLong Gold Antifade Reagent With DAPI (Invitrogen, ThermoFisher Scientific). Slides were stored at 4°C in the dark until imaging was performed by a Nikon histological microscope.

Flow Cytometric Analysis

To quantify the percentage of infiltrating immune cells at 24 hours from implantation, scaffolds were digested with collagenase I (2 mg/ml) (Life Technologies, ThermoFisher Scientific). Cell suspensions were filtered through 70-μm nylon mesh filters (BD Biosciences) to remove cell clumps and scaffold debris, spun at 500 g for 5 minutes, and fixed with 70% ethyl alcohol, and washed with fluorescence-activated cell sorting buffer (bovine serum albumin 0.1%). The percentage of CD45-positive cells was determined by using the PE-Cy7 directly conjugated mouse antirat CD45 antibody (Pharmingen, BD Biosciences). A minimum of 20,000 events per sample was analyzed using a BD LSR Fortessa cell analyzer (BD Biosciences). Post hoc data analysis was performed by using FCS Express (De Novo Software, Glendale, CA, https://www.denovosoftware.com/).

Chondrogenic and Osteogenic Induction and Assessment

The potential of CSCL to induce MSC differentiation toward the chondrogenic and osteogenic lineages was evaluated during a 21-day period in vitro. MSCs at passage 3 were seeded onto scaffolds (CL and CSCL) at a density of 10,000/cm^2. Cells on scaffolds were exposed to chondrogenic (StemPro Osteogenesis Differentiation Kit, Gibco, ThermoFisher Scientific) or osteogenic (StemPro Chondrogenesis Differentiation Kit) media, respectively, or maintained in standard media. In both cases, medium was changed every 3 days during a 21-day period. After 21 days in culture, differentiation was confirmed by chondrogenesis- and osteogenesis-associated gene analysis. Osteogenic differentiation was also assessed by quantifying the calcium deposited by using a commercial QuantiChrom Calcium Assay Kit (DICA-500; BioAssay Systems, Hayward, CA, https://www.bioassaysys.com), in accordance with the manufacturer's instructions.

Gene Expression Analysis

Total RNA was isolated from cells grown on scaffolds by homogenization in 1 ml of Trizol reagent (Life Technologies, ThermoFisher

Published Ahead of Print on March 24, 2016 as 10.5966/sctm.2015-0233.

Scientific) with a PowerGen 125 tissue homogenizer (ThermoFisher Scientific) and according to the manufacturer's instructions. For each sample, RNA concentration and purity were measured using a NanoDrop spectrophotometer (ND1000, NanoDrop, ThermoFisher Scientific). Treatment with DNAse (Sigma-Aldrich) was performed to avoid DNA contamination. cDNA was synthesized from 1 μg of total RNA using a Taqman Reverse Transcription reagents kit (Applied Biosystems, ThermoFisher Scientific, Branchburg, NJ). Amplifications were set on plates in a final volume of 10 μl and carried out using TaqMan Fast Advanced Master Mix (Applied Biosystems, ThermoFisher Scientific). The following target probes (Applied Biosystems, ThermoFisher Scientific) were used to evaluate the expression of the following markers.

Specific Lineage-Associated Markers

These markers included osteocalcin (*Bglap*; Rn00566386_g1), osteopontin (*Spp1*; Rn01449972_m1), and alkaline phosphatase (*Alp*; Rn01516028_m1) expression for osteogenesis and the SRY-related high-mobility group box transcription factor (*Sox9*; Rn01751069_mH), type 2 collagen (*Col2α1*; Rn01637087_m1), and aggrecan (*Acan*; Rn00573424_m1) for chondrogenesis.

Immunosuppression-Associated Markers

These markers included prostaglandin E synthase (*Pges;* Rn00572047_m1), cyclooxygenase-2 (*Cox-2*; Rn01483828_m1), inducible nitric oxide synthase (*iNos*; Rn00561646), and transforming growth factor-β (*Tgf-β*; Rn00572010_m1).

In Vivo Lymphocyte Apoptosis-Associated Markers

These markers included chemokine receptor type 5 (*Ccr5*; Rn00588629_m1), C-X-C chemokine receptor types 2 (*Cxcr2*; Rn02130551_s1) and 12 (*Cxcl12;* Rn01462853_m1), FAS ligand (*Faslg*; Rn00563754_m1), and interleukin-3 (*IL-3*; Rn01646318_g1).

Normalization of Data

Gene expression was normalized to the level of glyceraldehyde 3-phosphate dehydrogenase (*Gapdh; Rn01775763_g1*). For differentiation, data were compared with a control of cells cultured on CL scaffolds. For immunosuppression, values were normalized to those obtained from their respective control groups (unstimulated cells). Gene expression performed on ex vivo samples was evaluated compared with subcutaneous tissues with no inflammation (baseline).

Statistical Analysis

Statistical analysis was performed by using GraphPad Instat 3.00 for Windows (GraphPad Software, La Jolla, CA, http://www.graphpad.com/). Three replicates for each experiment (cell proliferation and distribution, gene expression, calcium deposition, PGE_2 and NO quantification assays, and PBMC test) were performed, and the results are reported as mean $\pm$ SD, with $p \leq .05$ used as a threshold for significance. One-way analysis of variance for multiple comparisons by the Student-Newman-Keuls multiple comparison test was used.

RESULTS

Scaffold Characterization

Figure 1A shows CL and CSCL scaffolds. The porous structure of scaffolds after freeze-drying has been determined by SEM imaging (Fig. 1A). The overall microstructure of all samples showed interconnected pores with boundaries that are defined by sheet-like structures of dense afibrillar collagen (CL) or more fibrillar collagen (CSCL). At higher magnification, it is clear that the presence of chondroitin sulfate imparts a more fibrous substructure. The copolymer CSCL has more widely interconnected pores, with mean diameters of 74 $\pm$ 11 μm, in comparison with bare collagen (CL), with a pore diameter of 62 $\pm$ 4 μm. CL presented a porosity of 81% and CSCL showed an overall higher porosity of 89%, as determined by capillary method. Figure 1B shows the average FTIR spectra of CL and CSCL. The vibration peak at approximately 1,400 cm^{-1}, correlating to a CH_2 side chain, is an important characteristic feature of collagen and was witnessed in all of the collagen-containing samples. Amide I (1,700–1,600 cm^{-1}) and amide II (1,600–1,500 cm^{-1}) are related to the stretching vibration of C = O bonds and to C–N stretching and N–H bending vibration, respectively. All samples contain C = O, C–N, and N–H bonds. Amide III region (approximately 1200–1300 cm^{-1}) is related to the C–N and C–C stretching, N–H bonds, and CH2 wagging from the glycine backbone and proline side chain. In the CSCL, amide I and amide II shift, showing a broader profile of their respective peaks. Amide III peaks (1,200, 1,237, and 1,280 cm^{-1}) shifted significantly in CSCL samples compared with CL, which may suggest the formation of bonding between afibrillar collagen and CS. At approximately 1,080 cm^{-1} (C–O stretching of carbohydrate residues in collagen and proteoglycans), approximately 845 cm^{-1} and 1,120 cm^{-1} (C–O-S stretching) and approximately 1,397 cm^{-1} (COO stretching of amino side chains).

TGA-DSC analysis assessed the actual link between CS and collagen by evaluating CSCL degradation and transitions compared with those of CL (Fig. 1 C). In particular, the DSC analysis evidenced substantial differences between CSCL and CL. Both materials underwent an endothermic reaction around 100°C (evaporation of the water moisture present in the material). Significant differences in the thermal transitions between CSCL and CL happened after 200°C of the heating ramp. Compared with CL, CSCL presented an exothermic transition at 259.42°C, corresponding to the degradation of the polysaccharide. TGA showed the presence of 7.4 wt% of CS in the CSCL sample. The swelling of CSCL scaffolds was significantly higher than that of the CL scaffold (Fig. 1D), mainly because of the slightly higher porosity and the presence of chondroitin sulfate, which allow it to retain its natural sponge effect as a result of its negative charge [57]. Finally, scaffold degradation kinetics was performed through lysozyme-containing PBS. Although neither scaffold incubated in PBS alone showed significant weight changes after the first 21 days, CL scaffolds incubated in lysozyme showed weight reduction after 7 days and a weight loss of almost 50% at the final time point. CSCL showed a lower degradation kinetic. The last time point showed a 72% weight loss.

AFM analysis was performed on CL and CSCL to evaluate the elastic properties of both scaffolds (Fig. 1F). A total of 1,305 and 991 Young's modulus values were considered on CL (blue bars in Fig. 1F) and CSCL (red bars in Fig. 1F), respectively. In CL, the data spread consists of 0.014–74.1 MPa, with 89% of the data population clustered below 5 MPa, where a distribution trend is clearly visible. With a distribution that is significantly different from normal (AD $p <$ .005), a median value of 1.36 $\pm$ 1.12 MPa was observed. CSCL data (red bars in Fig. 1F) presented a spread between 0.048 and 186 MPa, with two thirds of the data points organized in two distributions at low values ($<$3.15 MPa), whereas a third presented no visible trend,

Published Ahead of Print on March 24, 2016 as 10.5966/sctm.2015-0233.

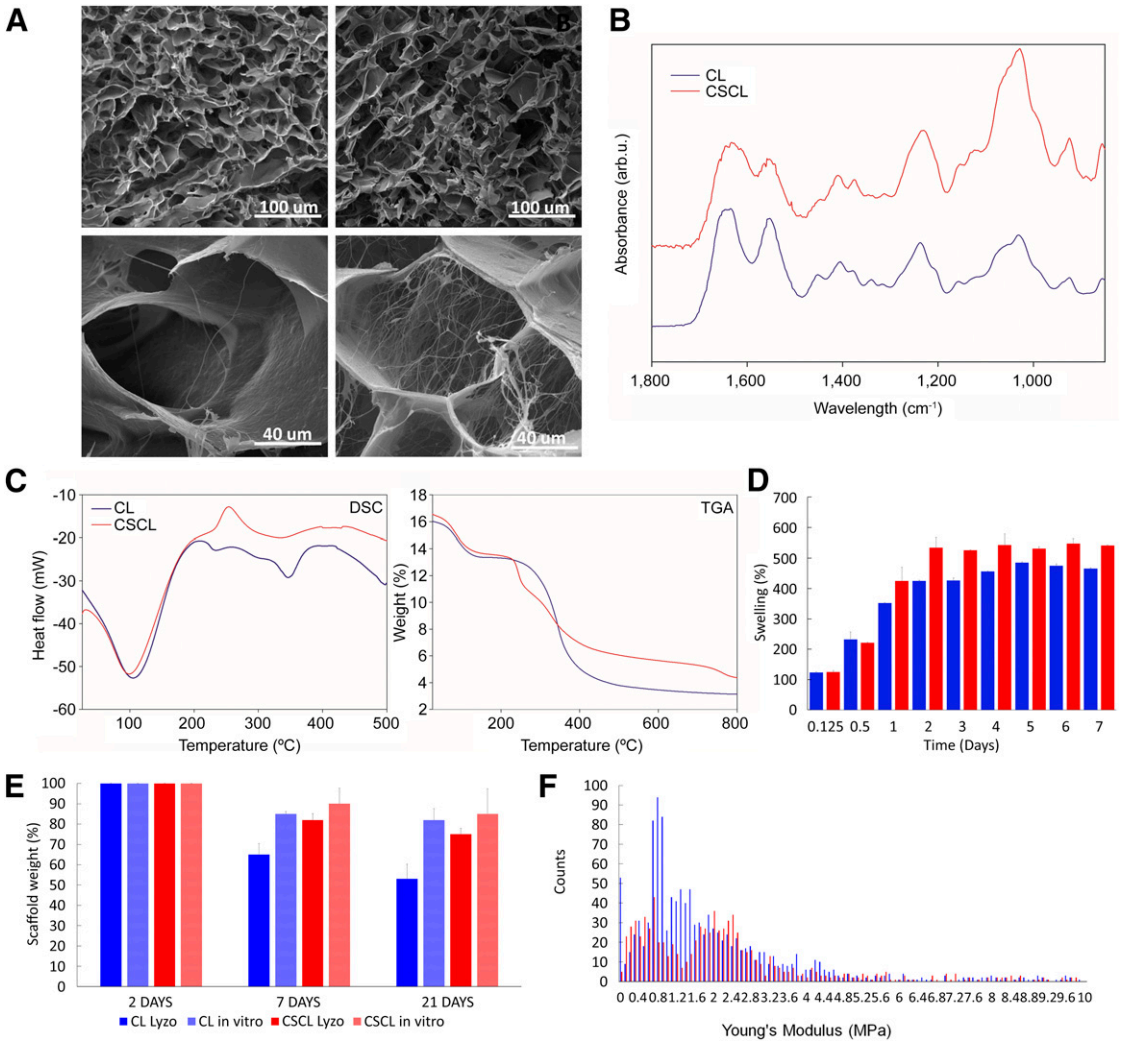

Figure 1. Structural and chemical characterization of the scaffolds. **(A):** Scanning electron microscopic images of CL and CSCL at different magnification. Scale bars are included in the figure. **(B):** Attenuated total reflection/Fourier transform infrared spectroscopy spectra of CL and CSCL. The spectra highlighted the presence of CS inside the collagen scaffold represented mainly on the sugar peaks that arise around 1,000 cm^{-1}. **(C):** Differential scanning calorimetry elucidated the thermal transitions of the CSCL respect to CL while thermal gravimetric analysis quantified the weight percentage of chondroitin sulfate in the scaffold. **(D):** The degradation percentage of CL (blue) and CSCL (red) scaffolds by lysozyme in phosphate-buffered saline solution. **(E):** Swelling characteristics in CL and CSCL over time. **(F):** Distribution of Young's modulus values for CL (blue) and CSCL (red). Abbreviation: CL, collagen scaffold; CSCL, chondroitin sulfate crosslinked onto a collagen-based scaffold.

with values ranging from 3.15 to 186 MPa. The median value of the first distribution was 0.64 ± 0.32 MPa, whereas the second peak, normally distributed (AD p = .005), had a median of 2.19 ± 0.42 MPa. Direct comparison of CL and CSCL distributions suggests that CS functionalization results in the introduction of two clearly distinct populations of mechanical properties compared with CL scaffolds. Both stiffness distributions in CSCL comprise a similar number of values; therefore, it is possible that they are similarly represented in the CSCL structure.

Cell Viability, Morphology, and Distribution

As revealed by confocal microscopy after 4 days of culture, cells infiltrated into the scaffold pores and covered 37.73% of the collagen surface in CL and 25.09% in CSCL scaffolds (Fig. 2A, lower magnification). Whereas in CL the cells organized in three-dimensional (3D) structures, in CSCL they aligned along the collagen fibers and distributed themselves homogeneously (Fig. 2A, higher magnification). By measuring the distance between the nuclei, we calculated that the cells were equidistant in CL and CSCL (26.74 ± 4.07 vs. 22.54 ± 5.53, respectively). The Live/Dead Assay demonstrated similar cell viability between CL and CSCL, which was assessed at approximately 99% (Fig. 2C). Alamar blue assay demonstrated that both CL and CSCL supported metabolically active cells growth during a period of 6 days (Fig. 2D).

Immunosuppressive Potential

To test the efficacy of the proposed material to help MSCs retain their immunosuppressive potential, cells grown onto CSCL and CL scaffolds were stimulated with the proinflammatory cytokine TNF-α (at the concentration of 10 and 50 ng/ml) for 48 hours. The secretion of immunosuppressive molecules did not increase

Published Ahead of Print on March 24, 2016 as 10.5966/sctm.2015-0233.

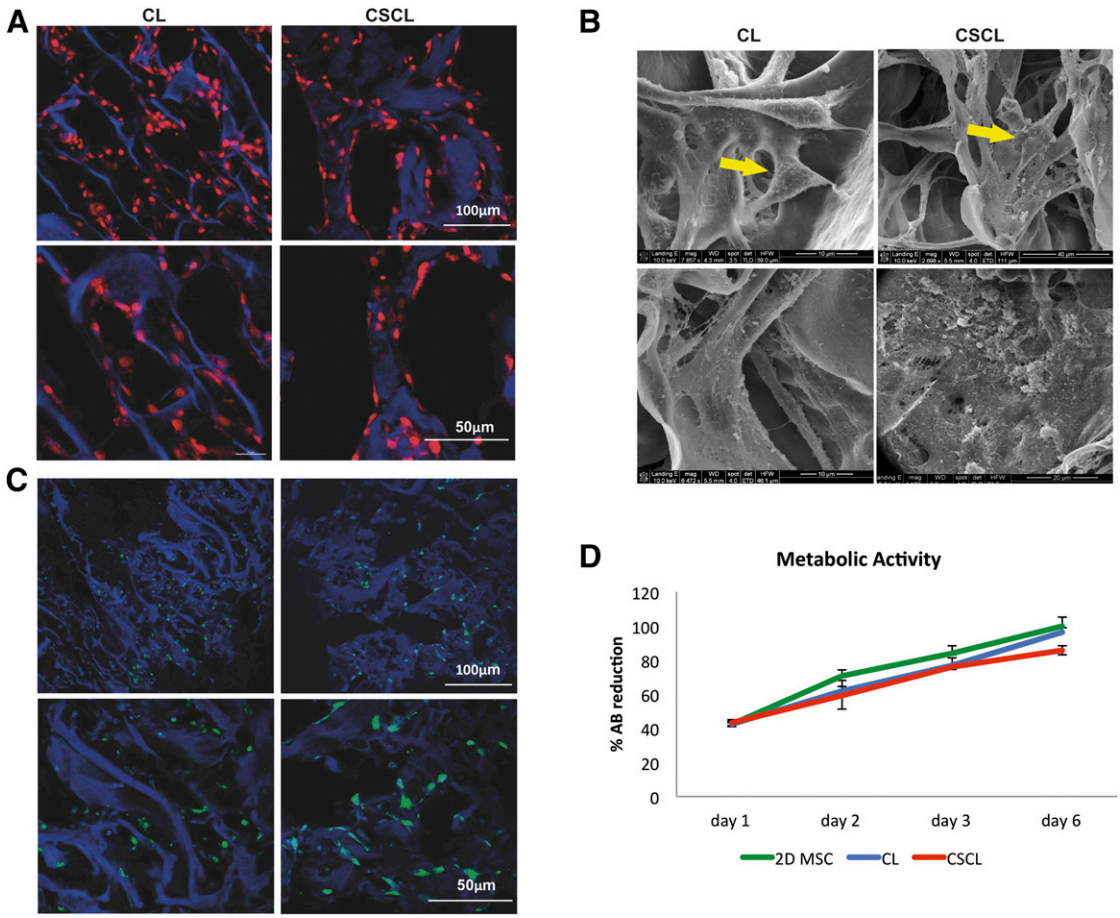

Figure 2. MSC spreading, viability, and proliferation. Confocal **(A)** and scanning electron microscopic (SEM) **(B)** images showing MSC spread onto CL and CSCL scaffolds at different magnifications. MSCs align along the walls of the scaffolds in the presence of chondroitin sulfate and organize in three-dimensional structures when grown onto CL **(A, B)**. SEM images reveal a greater production of microvesicles when MSCs are exposed to CSCL (arrows). Scale bars are included in the figure. CSCL and CL scaffolds support MSC viability **(C)** (Live/Dead assay) and proliferation **(D)** (Alamar blue assay). Temporal changes in the %AB are shown as representative of the presence of metabolically active cells over time. A cumulative increase in %AB reduction was found, reflecting ongoing cell proliferation. MSCs grown in two-dimensional conditions are also reported for comparison. Data are shown as mean of three independent biological replicates ± SD. Abbreviations: %AB, percentage of Alamar blue reduction; CL, collagen scaffold; CSCL, chondroitin sulfate crosslinked onto a collagen-based scaffold; MSC, mesenchymal stem cell.

when cells were stimulated with the lowest dose of TNF-α (10 ng/ml), nor was there a statistically significant difference in comparison with cells grown in 2D cultures under standard conditions (data not shown). The levels of PGE_2 released by cells grown in CSCL were decreased compared with CL in standard media ($p < .01$); although both CL/CSCL released significantly more PGE_2 than their 2D controls when stimulated, these values when stimulated were both near 1,500 pg/ml and did not differ significantly from one another (Fig. 3A). Compared with the unstimulated cells, *Pges* expression was 25- ± 7-fold higher in CSCL, with only a 2-increase in CL (Fig. 3C).

No significant differences were noted between the levels of NO produced in CSCL and CL in the absence of stimulation (Fig. 3B). In response to TNF-α stimulation, however, cells grown onto CL produced nearly identical amounts of NO compared with those cultured in 2D and standard conditions, whereas cells grown onto CSCL scaffolds released significantly higher amounts ($p < .01$) (Fig. 3B). Concomitantly, a significant increase in the expression of *iNos* (6.07 ± 0.25) was observed in comparison with 2D MSC and CL: 2 ± 0.35 and 2.89 ± 0.29, respectively. A similar trend in molecular upregulation was seen for *Cox2* and *Tgf-β* as well. Stimulated cells produced a 13- ± 0.35-fold and 3.8- ± 0.04-fold increase in *Cox-2* expression at 48 hours in CSCL and CL, respectively. *Tgf-β* expression did not significantly differ between CL and 2D MSCs but was greatly increased in CSCL (13 ± 0.5). Consistent with these previous findings, when their immunosuppressive potential was evaluated in a lymphocyte reaction assay, both CL and CSCL inhibited the proliferation of PHA-stimulated PBMCs after 3 days of coculture. However, as shown in Figure 3D, the inhibitory effect was greater in MSCs grown onto CSCL scaffolds compared with CL, showing a 42% decrease in PBMC proliferation; in contrast, it was approximately 23% in CL.

In Vivo Studies

We further examined the immunosuppressive effect of CSCL and CL in vivo. Animals did not experience complication from the surgical operation. Histologically stained sections reveal that after 24 hours infiltration of immune cells were reduced in CSCL compared with CL (Fig. 4A). Flow cytometric analysis revealed a five-fold decrease in the percentage of CD45-positive cells in CSCL than CL (Fig. 4B). These data were confirmed by immunohistochemistry,

Published Ahead of Print on March 24, 2016 as 10.5966/sctm.2015-0233.

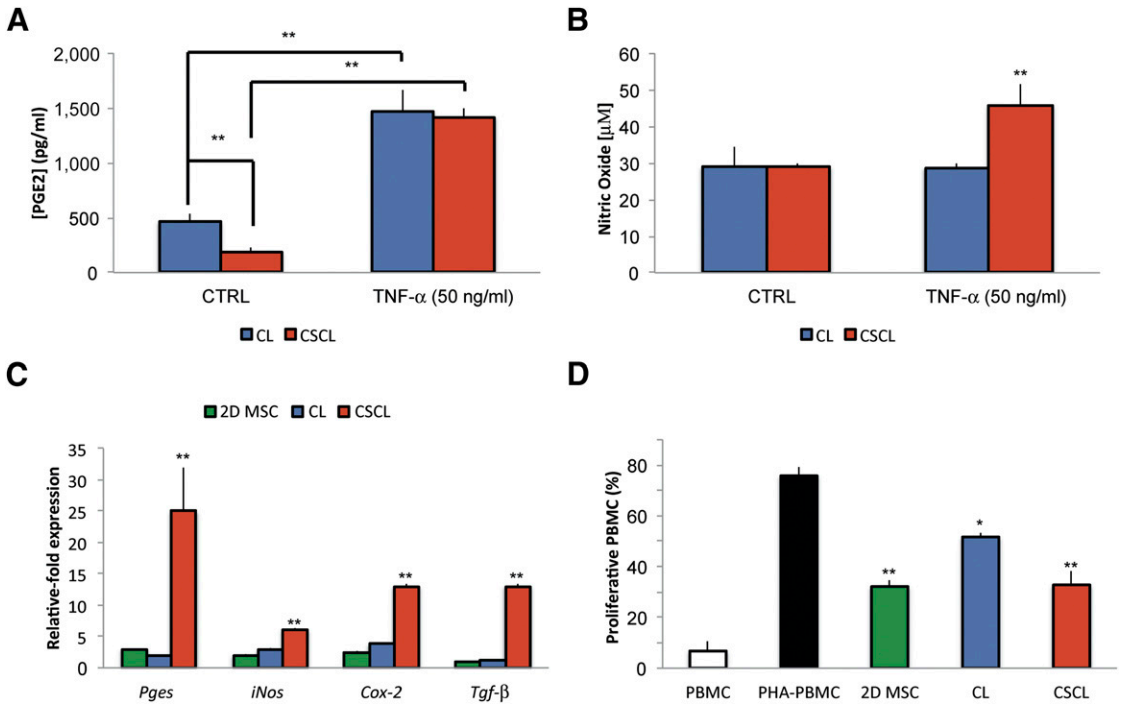

Figure 3. Role of CSCL in supporting MSC immunosuppressive potential in vitro. MSCs secrete various factors, such as PGE_2, nitric oxide, and transforming growth factor-β. PGE_2 **(A)** and nitric oxide **(B)** production by MSCs cultured onto CL and CSCL in response to stimulation with the proinflammatory cytokine TNF-α (50 ng/ml) at 48 hours. Asterisks depict highly significant (**, $p < .01$) differences compared with cells grown in standard media. **(C):** Comparison between MSCs grown onto CL and CSCL for the expression of *Pges*, *iNos*, *Cox-2* and *Tgf-β* after 48 hours of stimulation. Data are represented as fold-change compared with the expression levels found in the untreated cells ($n = 3$; **, $p < .01$). **(D):** Effect of MSCs grown in two dimensions or onto CL (CL) or CSCL (CSCL) on the proliferation of stimulated PBMC after 72 hours of coculture. For comparison the percentage of proliferative PBMCs in the presence (PHA-PBMC) and absence (PBMC) of PHA is also reported. Data represent the mean ± SD of three independent experiments. Asterisks depict highly significant (**, $p < .01$) and significant (*, $p < .05$) differences compared with stimulated PBMCs. Abbreviations: 2D MSC, two-dimensional mesenchymal stem cell; CL, collagen scaffold; CSCL, chondroitin sulfate cross-linked onto a collagen-based scaffold; CTRL, control; MSC, mesenchymal stem cell; PBMC, peripheral blood mononuclear cell; PGE_2, prostaglandin E_2; PHA-PBMC, phytohemagglutinin peripheral blood mononuclear cell; TNF-α, tumor necrosis factor-α.

which showed a negligible presence of CD3+ cells inside the CSCL in comparison with CL (Fig. 4C). Among the genes studied, those associated with inflammatory cell apoptotic processes (*Cxcr2*, *Cxcl12*, *Faslg*, and *IL-3*) were significantly ($p < .01$) increased in CSCL (Fig. 4D).

Osteogenic and Chondrogenic Differentiation

The osteogenic and chondrogenic potential of our scaffolds was assessed during a 21-day period. MSCs on scaffolds were exposed to chondrogenic media or kept in standard media. The highly upregulated expression of specific chondrogenesis-associated genes, such as *Sox9*, *Acan*, and *Col2α1* (Fig. 5) confirmed that differentiation toward the chondrogenic lineage in both uninduced and induced cells grown in CSCL occurred. In particular, the expression of the transcription factor *Sox9* was increased 4.12- ± 0.04-fold when cells were cultured onto CSCL scaffolds without the addition of any supplement in the media compared with CL. It reached higher values when cells were properly induced with the chondrogenic media (8.97 ± 0.34). Accordingly, compared with cells grown onto CL scaffolds, *Acan* expression increased 3.06- ± 0.21-fold when the CS was crosslinked to the collagen in total absence of chondrogenic supplements and increased to 4.06 ± 0.18 when properly induced. Accordingly, *Col2α1* expression was found 5.43- ± 0.52-fold higher in CSCL compared with CL, but this value did not change when media was supplemented with chondrogenesis-inducing factors.

In the absence of osteogenic media, CSCL scaffolds did not show any osteogenic potential. However, the synergistic action of the CSCL scaffold structure and the inducing media did exhibit a significantly enhanced osteogenic effect induced as confirmed by the upregulation of specific osteogenesis-associated genes (Fig. 6A). After induction, alkaline phosphatase (*Alp*) expression increased 2.35- ± 0.18-fold in cells grown on CSCL compared with CL. Similarly, *Bglap* expression was 4.5 ± 0.23 times increased in CSCL, whereas the expression of osteopontin (*Spp1*) was only 1.89- ± 0.07-fold higher in comparison with cells grown on CL scaffolds. When induced, the two experimental groups showed a 3-fold increase in the concentration of minerals deposited in the media, without any statistically significant differences between the groups (Fig. 6B).

Discussion

The extracellular matrix is the key factor in maintaining homeostasis of a normal tissue because it helps resident cells in several specific functions, including adhesion, migration, proliferation, and differentiation [58]. An effective biomaterial-based regenerative strategy requires not only the matching of tissue-specific

Published Ahead of Print on March 24, 2016 as 10.5966/sctm.2015-0233.

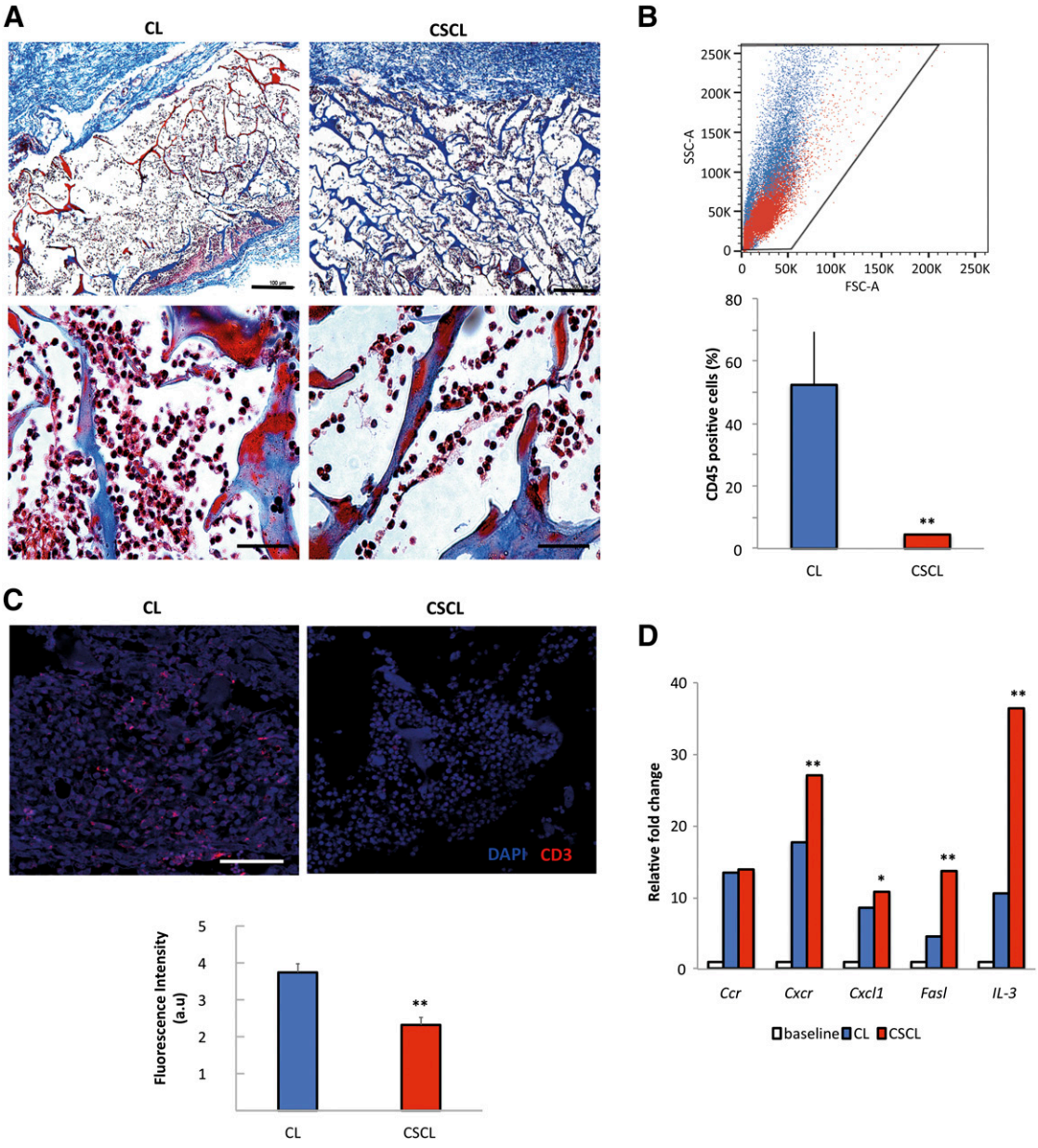

Figure 4. CSCL immunosuppressive potential when subcutaneously implanted in rats in vivo for 24 hours. **(A):** Masson's trichrome-stained sections of CL and CSCL ex vivo (original magnification, ×4 and ×40). Scale bars = 100 μm for ×4 magnification and 10 μm for ×40 magnification. **(B):** Representative morphological plots showing cells harvested from CL (blue) and CSCL (red) scaffolds. Histograms represent the percentage of CD45-positive cells identified at 24 hours. Asterisks depict highly significant (**, $p < .01$) differences between CL and CSCL. **(C):** Immunofluorescence staining of CD3+ (red) infiltrate the scaffold in subcutaneous implant model. Scale bar = 50 μm. Data are quantified as mean fluorescence intensity with Nikon Element software. Asterisks depict significant (**, $p < .01$) differences between CL and CSCL. **(D):** Quantitative polymerase chain reaction for the expression of genes involved in inflammatory cell apoptotic processes (*Cxcr2*, *Cxcl12*, *Faslg*, and *IL-3*). Data are represented as fold-change compared with the expression levels found in subcutaneous tissues with no inflammation (baseline) ($n = 3$; **, $p < .01$; *, $p < .05$). Abbreviations: au, arbitrary unit; CL, collagen scaffold; CSCL, chondroitin sulfate crosslinked onto a collagen-based scaffold; DAPI, 4′,6-diamidino-2-phenylindole; FSC-A, forward scatter pulse area; SSC-A, side scatter pulse area.

structural and functional cues but also the control of the host immune response to the biomaterial of choice [59]. In particular, in the case of trauma or degenerative inflammatory diseases, cartilage tends to progressively degrade because of the low regenerative capacity of the natural tissue. To solve this issue, several tissue-engineered approaches using biopolymeric scaffolds that mimic the ECM of cartilage have been explored [40–42] so far, although none of them has proven capable of conquering the subsequent host immune response. With this in mind, we sought to develop a biomaterial that can fine-tune the inflammatory response after implantation and at the same time recapitulate the chondrogenic niche.

Because of the proven immunomodulatory properties of CS [33] and the fact that it is one of the most represented components of cartilage [60], we integrated CS into a collagen-based scaffold to create a desirable environment for MSC to exert

Published Ahead of Print on March 24, 2016 as 10.5966/sctm.2015-0233.

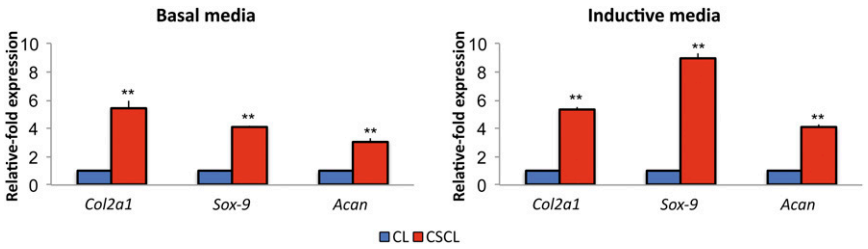

Figure 5. Chondrogenic differentiation in vitro. Mesenchymal stem cells were grown onto CL and CSCL for a 21-day period in basal or inductive media. Quantitative polymerase chain reaction analysis for the chondrogenesis (*Sox9*, *Col2a1*, *Acan*)-associated markers. Expression levels normalized to the reference gene (*Gapdh*). Data are represented as fold-change compared with expression cells grown on CLs. Asterisks depict highly significant (**, $p < .01$) differences. Abbreviation: CL, collagen scaffold; CSCL, chondroitin sulfate crosslinked onto a collagen-based scaffold.

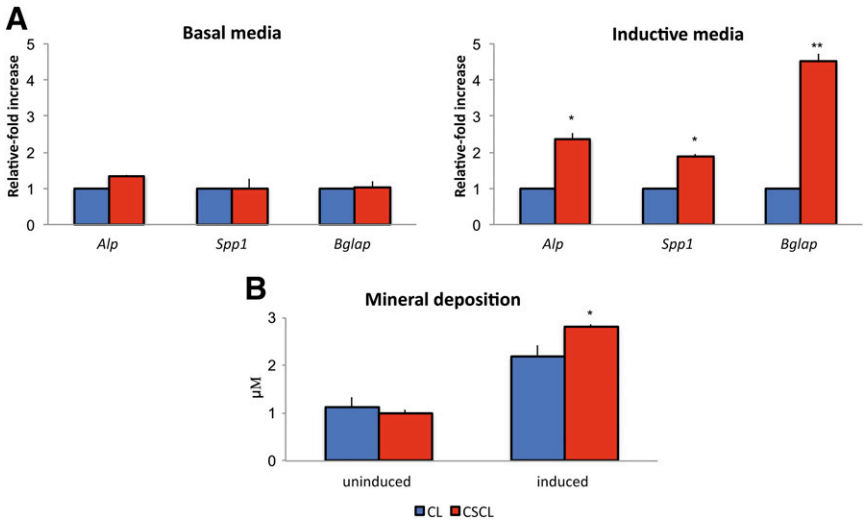

Figure 6. Osteogenic differentiation in vitro. Mesenchymal stem cells were grown onto CL and CSCL for a 21-day period in basal or inductive media. **(A):** Quantitative polymerase chain reaction analysis for the osteogenic (*Alp*, *Spp1*, *Bglap*)-associated markers. Expression levels normalized to the reference gene (*Gapdh*). Data are represented as fold-change compared with expression cells grown on CLs. **(B):** Mineral deposition (μM) evaluated after 21 days of culture onto CL and CSCL whether cells were exposed to inductive media. Values are mean ± SD. $n = 3$. Asterisks depict significant (*, $p < .05$) and highly significant (**, $p < .01$) differences between CL and CSCL. Abbreviation: CL, collagen scaffold; CSCL, chondroitin sulfate crosslinked onto a collagen-based scaffold.

their protective and regenerative effects. MSCs hold an inherent immunoregulatory potential and elicit immunosuppressive effects in several situations [43]; they are able to interfere with a variety of immune cell functions (i.e., cytokine secretion and cytotoxicity of T and NK cells, B cell maturation and antibody secretion, dendritic cell maturation and activation, and well as antigen presentation) by means of direct cell-to-cell interactions or soluble factor secretion, such as NO and PGE_2 [61]. In this scenario, we exposed MSCs grown onto CL and CSCL to a proinflammatory environment to evaluate the capability of the system to help MSCs retain their immunosuppressive effect without inducing a material-dependent stress.

When activated, MSCs on CSCL more vigorously reacted to stimulation with TNF-α (50 ng/ml). A marked accumulation ($p < .01$) of NO was observed only when cells were cultured onto CSCL scaffold, whereas CL alone was essentially noninducible for NO release. In addition, although the absolute levels of PGE_2 upon induction were similar between CL and CSCL, the percentage change baseline was significantly increased in CSCL because it released much lower basal levels of PGE_2 ($p < .05$). Interestingly, the basal levels of PGE_2 found in CSCL were even lower than those observed in CL ($p < .05$). This suggested that the environment created by CSCL resulted in less stress for cells that need to be activated to exert their immunomodulation potential, mainly because of the architecture, composition, and mechanical properties of the material, which are different between CL and CSCL. These data were corroborated by the significant increase in the expression of *iNos*, *Pges*, *Cox-2*, and *Tgf-β*. Because the production of such molecules ultimately leads to the inhibition of T cell proliferation [62, 63], we confirmed the preliminary observations testing the effect of CSCL in supporting the inhibition of PHA-stimulated PBMC proliferation in a cell-cell contact assay. The functional study confirmed the greater immunosuppressive potential of MSCs grown onto CSCL yet suggested a lower immunogenic capability of MSCs when CS is not included in the system.

To further validate our in vitro results, we evaluated the immunosuppressive nature of CSCL scaffold via implantation in a subcutaneous model in vivo. As revealed by histological staining and immunofluorescence, infiltration of CD3+ cells at 24 hours was lower in CSCL than CL, thus confirming the intrinsic immunosuppressive effect of the proposed CSCL scaffold. Flow cytometric analysis quantifiably supports the histological trend showing a

Published Ahead of Print on March 24, 2016 as 10.5966/sctm.2015-0233.

significant reduction in the percentage of CD45+ cells (including precursor cells and mature lymphocytes, granulocytes, and dendritic cells), passing from 50% ± 16.97% in CL to 4.5% ± 0.28% in CSCL. We can hypothesize that the reduced number of CD3+ cells observed in CSCL compared with CL is a relative decrease. In fact, it could be mainly due to the different process activated by CS, together with the architecture provided to the scaffold by its presence, and its ability able to exert its anti-inflammatory effect by recruiting a functionally different cell population compared with bare CL.

To better understand the mechanisms involved in such a reduction, we analyzed some of the genes associated with a diminished proinflammatory cascade, leading to the recruitment of less inflammatory cells in the area of the implant. Our data confirmed the supposed immunosuppression mediated by the material itself because a greater upregulation of those genes was revealed by quantitative PCR when CSCL was implanted.

After establishing the immunomodulatory properties of our CSCL scaffold, we examined its proficiency in driving chondrogenic and osteogenic differentiation of naïve MSCs. Specifically, we tested the ability of our system to recreate the stimuli found in the chondrogenic niche. We observed that the CS cross-linking to the collagen provided MSCs with mechanical and biochemical cues required to induce spontaneous differentiation toward the chondrogenic lineage. Without the requirement of external influence from differentiative medium, MSCs grown on CSCL for 21 days expressed high levels of chondrogenesis-associated genes. In particular, the Sry-related high-mobility group box transcription factor (*Sox9*) is an early marker whose expression regulates the rate of chondrocyte differentiation by controlling the expression of specific genes (type 2 collagen [*Col2a1*] and aggrecan [*Acan*]) [64].

The same phenomenon was not witnessed in control CL scaffolds, suggesting that the CS immobilized to our CSCL scaffold is necessary and could be sufficient for such cellular differentiation. The expression profile observed was similar to or even greater than that found when cells were chemically induced with commercial differentiation medium (data not shown).

Data obtained are consistent with prior literature, confirming the capability of CS to enhance chondrocyte proliferation and maturation [65–67]. As suggested by the FTIR spectra, chondrogenesis was likely achieved because of the biomimetic ultrastructure of the CSCL; it was similar to that seen in natural aggrecan [68]. As mentioned previously, aggrecan is considered the constituent molecule of support tissues and, together with collagen fibers, contributes to the cohesion and improved mechanical features of cartilage [60].

The functionalization of our collagen-based scaffold with chondroitin sulfate, as well as the crosslinking procedure, verified by TGA, DSC, and FTIR, did slightly affect the porosity and the mechanical features of the material. Porosity is considered a key factor in the success of regenerative biomaterial tissue integration because it allows for the proper organization of cells seeded/infiltrating into the scaffold [24].

MSCs grown onto CSCL aligned along the pores in the three-dimensional scaffolds, whereas those seeded onto CL scaffold appeared to form clusters, thus revealing a higher degree of cellular adhesion to the microenvironment provided by CSCL that is crucial for cytoskeletal organization and cell specification [69, 70]. In addition, MSCs grown on CSCL showed higher numbers of vesicles, hypothesized to be relevant for an enhanced cell-cell communication activity. In fact, extracellular vesicles have important roles in the regulation of the crosstalk between MSCs and immune cells, mediating their inflammatory stimulation or suppression together with freely secreted molecules [71]. Addition of chondroitin sulfate increases stiffness heterogeneity in CSCL scaffolds, with two regions with lower and higher stiffness compared with CE scaffolds (Fig. 1E). It is unclear how the change in stiffness is related to scaffolds' 3D structure. Regions of higher stiffness may be localized in the areas where the chondroitin sulfate web inside the pores significantly stabilizes the sheet-like structures (Fig. 1A). Although areas of lower stiffness may be found in those areas with a significant increase in pore diameter, longer sheet-like structures that surround pores are more elastic in their midareas compared with shorter ones. As previously demonstrated, low stiffness facilitates a significant upregulation in SOX9 [72], and the region of lower stiffness in CSCL, compared with CL, may play a role in the upregulation of SOX9 observed in the present work (Fig. 5).

Although it has been proposed that collagen type I itself induces the differentiation of osteoprogenitor cells into osteoblast-like cells [73], no osteogenic differentiation was observed when cells were grown onto CL or CSCL in basal media, suggesting that the scaffold did not provide the minimum necessary chemical and mechanical cues for cells to undergo osteoblastogenesis. When appropriately stimulated, however, the expression of the osteogenesis-associated markers (*Alp*, *Spp1*, *Bglap*) was statistically significantly increased in CSCL compared with CL, thus suggesting potential use of the proposed scaffold for approaches aimed at restoring the osteochondral region of long bones or articular surfaces.

Conclusion

The complex interaction between biomaterials and the host cellular environment is poorly defined. The data we have presented prove that fine alterations in the physicochemical structure of biotherapeutic moieties can concurrently direct the immune system away from immunologic rejection and stimulate the body to essentially heal itself via terminal MSC differentiation toward the tissue of interest. An implantable scaffold capable of initiating regeneration while being incorporated into the tissue would avoid many of the current limitations of implanted prostheses and could represent the Holy Grail for regenerative medicine applications. The immunomodulatory strategy we propose, based on a CS-functionalized collagen scaffold, is a good example of a biomimetic material able to recapitulate the cartilage environment while reducing inflammation at the site of implant.

Acknowledgments

This work was supported by the Cullen Trust for Health Care Foundation for stem cell plasticity studies (Project ID: 18130014) and the Brown Foundation (Project ID: 18130011) to E.T. E.T.'s fellowship was supported by the Italian Ministry of Health (GR-2010-2318370). Partial funds were obtained from the Ernest Cockrell Jr. Presidential Distinguished Chair (M.F.).

Published Ahead of Print on March 24, 2016 as 10.5966/sctm.2015-0233.

Author Contributions

B.C.: study conception and design, collection and assembly of data, data analysis and interpretation, manuscript writing; F.T.: design, synthesis and characterization of study materials, collection and analysis of data, manuscript writing; S.M.: collection and analysis of TGA, DSC, and confocal laser microscopy data, manuscript editing; J.V.E: in vivo study design and operations, specimen collection, manuscript editing; F.C.: in vivo operations, specimen collection, collection of data; L.W.F. and S.A.G.: mechanical characterization of the materials; M.F.: administrative support; B.K.W.: financial support; E.T.: financial and administrative support, final approval of the manuscript.

Disclosure of Potential Conflicts of Interests

F.T. has compensated employment, intellectual property rights, and research funding. The other authors indicated no potential conflicts of interest.

References

1 Ahmed TA, Hincke MT. Strategies for articular cartilage lesion repair and functional restoration. Tissue Eng Part B Rev 2010;16:305–329.

2 Buckwalter JA, Saltzman C, Brown T. The impact of osteoarthritis: Implications for research. Clin Orthop Relat Res 2004;427(suppl):S6–S15.

3 Bos PK. van Melle MLvan Osch G. Articular cartilage repair and the evolving role of regenerative medicine. Open Access Surg 2010;3: 109–122.

4 Hamel MB, Toth M, Legedza A et al. Joint replacement surgery in elderly patients with severe osteoarthritis of the hip or knee: decision making, postoperative recovery, and clinical outcomes. Arch Intern Med 2008;168:1430–1440.

5 Schrama JC, Espehaug B, Hallan G et al. Risk of revision for infection in primary total hip and knee arthroplasty in patients with rheumatoid arthritis compared with osteoarthritis: A prospective, population-based study on 108,786 hip and knee joint arthroplasties from the Norwegian Arthroplasty Register. Arthritis Care Res (Hoboken) 2010;62:473–479.

6 Dixon T, Shaw M, Ebrahim S et al. Trends in hip and knee joint replacement: Socioeconomic inequalities and projections of need. Ann Rheum Dis 2004;63:825–830.

7 Ingham E, Fisher J. The role of macrophages in osteolysis of total joint replacement. Biomaterials 2005;26:1271–1286.

8 Mahmoudifar N, Doran PM. Chondrogenesis and cartilage tissue engineering: The longer road to technology development. Trends Biotechnol 2012;30:166–176.

9 Boehler RM, Graham JG, Shea LD. Tissue engineering tools for modulation of the immune response. Biotechniques 2011;51:239–240, 242, 244 passim.

10 Murphy WL, McDevitt TC, Engler AJ. Materials as stem cell regulators. Nat Mater 2014; 13:547–557.

11 Anderson JM, Rodriguez A, Chang DT. Foreign body reaction to biomaterials. Semin Immunol 2008;20:86–100.

12 Avula MN, Rao AN, McGill LD et al. Modulation of the foreign body response to implanted sensor models through device-based delivery of the tyrosine kinase inhibitor, masitinib. Biomaterials 2013;34:9737–9746.

13 Sridharan R, Cameron AR, Kelly DJ et al. Biomaterial based modulation of macrophage polarization: A review and suggested design principles. Mater Today 2015;18:313–325.

14 Bos PK, Kops N, Verhaar JA et al. Cellular origin of neocartilage formed at wound edges of articular cartilage in a tissue culture experiment. Osteoarthritis Cartilage 2008; 16:204–211.

15 van Osch GJ, Brittberg M, Dennis JE et al. Cartilage repair: Past and future–lessons for regenerative medicine. J Cell Mol Med 2009;13: 792–810.

16 Shapiro F, Koide S, Glimcher MJ. Cell origin and differentiation in the repair of full-thickness defects of articular cartilage. J Bone Joint Surg Am 1993;75:532–553.

17 Wilusz RE, Sanchez-Adams J, Guilak F. The structure and function of the pericellular matrix of articular cartilage. Matrix Biol 2014; 39:25–32.

18 Keeney M, Lai JH, Yang F. Recent progress in cartilage tissue engineering. Curr Opin Biotechnol 2011;22:734–740.

19 Parenteau-Bareil R, Gauvin R, Berthod F. Collagen-based biomaterials for tissue engineering applications. Materials (Basel) 2010;3: 1863–1887.

20 Kiani C, Chen L, Wu YJ et al. Structure and function of aggrecan. Cell Res 2002;12:19–32.

21 Toh WS, Lee EH, Guo X-M et al. Cartilage repair using hyaluronan hydrogel-encapsulated human embryonic stem cell-derived chondrogenic cells. Biomaterials 2010;31:6968–6980.

22 Filardo G, Kon E, Roffi A et al. Scaffold-based repair for cartilage healing: A systematic review and technical note. Arthroscopy 2013; 29:174–186.

23 Chen F, Yoo JJ, Atala A. Acellular collagen matrix as a possible "off the shelf" biomaterial for urethral repair. Urology 1999;54:407–410.

24 Hollister SJ. Porous scaffold design for tissue engineering. Nat Mater 2005;4:518–524.

25 Chandran PL, Horkay F. Aggrecan, an unusual polyelectrolyte: Review of solution behavior and physiological implications. Acta Biomater 2012;8:3–12.

26 Schnabelrauch M, Scharnweber D, Schiller J. Sulfated glycosaminoglycans as promising artificial extracellular matrix components to improve the regeneration of tissues. Curr Med Chem 2013;20:2501–2523.

27 Sugahara K, Mikami T, Uyama T et al. Recent advances in the structural biology of chondroitin sulfate and dermatan sulfate. Curr Opin Struct Biol 2003;13:612–620.

28 Liang WH, Kienitz BL, Penick KJ et al. Concentrated collagen-chondroitin sulfate scaffolds for tissue engineering applications. J Biomed Mater Res A 2010;94:1050–1060.

29 Volpi N. Anti-inflammatory activity of chondroitin sulphate: New functions from an old natural macromolecule. Inflammopharmacology 2011; 19:299–306.

30 Vallieres M, Du Souich P. Modulation of inflammation by chondroitin sulfate. Osteoarthritis Cartilage 2010;18:S1–S6.

31 du Souich P, García AG, Vergés J et al. Immunomodulatory and anti-inflammatory effects of chondroitin sulphate. J Cell Mol Med 2009;13 (8a):1451–1463.

32 Linhardt RJ, Toida T. Role of glycosaminoglycans in cellular communication. Acc Chem Res 2004;37:431–438.

33 Akiyama H, Sakai S, Linhardt RJ et al. Chondroitin sulphate structure affects its immunological activities on murine splenocytes sensitized with ovalbumin. Biochem J 2004;382:269–278.

34 Bali J-P, Cousse H, Neuzil E. Biochemical basis of the pharmacologic action of chondroitin sulfates on the osteoarticular system. Semin Arthritis Rheum 2001;31:58–68.

35 Kelly GS. The role of glucosamine sulfate and chondroitin sulfates in the treatment of degenerative joint disease. Altern Med Rev 1998; 3:27–39.

36 Monfort J, Pelletier J-P, Garcia-Giralt N et al. Biochemical basis of the effect of chondroitin sulphate on osteoarthritis articular tissues. Ann Rheum Dis 2008;67:735–740.

37 Ishizeki K, Hiraki Y, Kubo M et al. Sequential synthesis of cartilage and bone marker proteins during transdifferentiation of mouse Meckel's cartilage chondrocytes in vitro. Int J Dev Biol 1997;41:83–89.

38 McCarty MF, Russell AL, Seed MP. Sulfated glycosaminoglycans and glucosamine may synergize in promoting synovial hyaluronic acid synthesis. Med Hypotheses 2000;54:798–802.

39 Yannas IV, Burke JF, Gordon PL et al. Design of an artificial skin. II. Control of chemical composition. J Biomed Mater Res 1980;14:107–132.

40 Marijnissen WJ, van Osch GJ, Aigner J et al. Alginate as a chondrocyte-delivery substance in combination with a non-woven scaffold for cartilage tissue engineering. Biomaterials 2002;23:1511–1517.

41 Marijnissen WJ, van Osch GJ, Aigner J et al. Tissue-engineered cartilage using serially passaged articular chondrocytes. Chondrocytes in alginate, combined in vivo with a synthetic (E210) or biologic biodegradable carrier (DBM). Biomaterials 2000;21:571–580.

42 Oliveira JT, Crawford A, Mundy JM et al. A cartilage tissue engineering approach combining starch-polycaprolactone fibre mesh scaffolds with bovine articular chondrocytes. J Mater Sci Mater Med 2007;18:295–302.

43 Caplan AI, Sorrell JM. The MSC curtain that stops the immune system. Immunol Lett 2015;168:136–139.

44 Trabanelli S, La Manna F, Romano M et al. The human mesenchymal stromal cell-derived osteocyte capacity to modulate dendritic cell functions is strictly dependent on the culture system. J Immunol Res 2015;2015:526195.

45 Murphy MB, Moncivais K, Caplan AI. Mesenchymal stem cells: Environmentally

Published Ahead of Print on March 24, 2016 as 10.5966/sctm.2015-0233.

responsive therapeutics for regenerative medicine. Exp Mol Med 2013;45:e54.

46 Yoo JU, Barthel TS, Nishimura K et al. The chondrogenic potential of human bone-marrow-derived mesenchymal progenitor cells. J Bone Joint Surg Am 1998;80:1745–1757.

47 Lange-Consiglio A, Corradetti B, Bizzaro D et al. Characterization and potential applications of progenitor-like cells isolated from horse amniotic membrane. J Tissue Eng Regen Med 2012;6:622–635.

48 Lange-Consiglio A, Maggio V, Pellegrino L et al. Equine bone marrow mesenchymal or amniotic epithelial stem cells as feeder in a model for the in vitro culture of bovine embryos. Zygote 2012;20:45–51.

49 Corradetti B, Meucci A, Bizzaro D et al. Mesenchymal stem cells from amnion and amniotic fluid in the bovine. Reproduction 2013; 145:391–400.

50 Willerth SM, Sakiyama-Elbert SE. Combining stem cells and biomaterial scaffolds for constructing tissues and cell delivery. In: StemBook. Cambridge, MA: Harvard Stem Cell Institute, 2008.

51 Martino G, Bacigaluppi M, Peruzzotti-Jametti L. Therapeutic stem cell plasticity orchestrates tissue plasticity. Brain 2011;134:1585–1587.

52 Tan H, Wu J, Lao L et al. Gelatin/chitosan/hyaluronan scaffold integrated with PLGA microspheres for cartilage tissue engineering. Acta Biomater 2009;5:328–337.

53 Dong Z, Wejinya UC, Zhu Y et al. Force measurement study of engineered collagen-chitosan scaffold using atomic force microscopy. Presented at Nano/Molecular Medicine and Engineering (NANOMED), 2010 IEEE 4th International Conference; December 5–9, 2010; Hong Kong.

54 Russo L, Battocchio C, Secchi V et al. Thiol-ene mediated neoglycosylation of collagen patches: a preliminary study. Langmuir 2014;30:1336–1342.

55 Soleimani M, Nadri S. A protocol for isolation and culture of mesenchymal stem cells from mouse bone marrow. Nat Protoc 2009;4: 102–106.

56 Hegyi B, Kudlik G, Monostori E et al. Activated T-cells and pro-inflammatory cytokines differentially regulate prostaglandin E2 secretion by mesenchymal stem cells. Biochem Biophys Res Commun 2012;419:215–220.

57 Yung S, Chan TM. Glycosaminoglycans and proteoglycans: Overlooked entities? Perit Dial Int 2007;27(suppl 2):S104–S109.

58 Cox TR, Erler JT. Remodeling and homeostasis of the extracellular matrix: Implications for fibrotic diseases and cancer. Dis Model Mech 2011;4:165–178.

59 Brown BN, Sicari BM, Badylak SF. Rethinking regenerative medicine: A macrophage-centered approach. Front Immunol 2014;5:510.

60 Alberts B, Johnson A, Lewis J et al. The extracellular matrix of animals. In: Molecular Biology of the Cell. 4th ed. New York, NY: Garland Science, 2002.

61 Nehlin J, Isa A, Barington T. Immunogenicity and immune-modulating properties of human stem cells. In: Gholamrezanezhad A, ed. Stem Cells in Clinic and Research. Rijeka, Croatia: InTech, 2011.

62 Zinöcker S, Vaage JT. Rat mesenchymal stromal cells inhibit T cell proliferation but not cytokine production through inducible nitric oxide synthase. Front Immunol 2012;3:62.

63 Zinöcker S, Wang MY, Rolstad B et al. Mesenchymal stromal cells fail to alleviate experimental graft-versus-host disease in rats transplanted with major histocompatibility complex-mismatched bone marrow. Scand J Immunol 2012;76:464–470.

64 Akiyama H, Kamitani T, Yang X et al. The transcription factor Sox9 is degraded by the ubiquitin-proteasome system and stabilized by a mutation in a ubiquitin-target site. Matrix Biol 2005;23:499–505.

65 Buma P, Pieper JS, van Tienen T et al. Cross-linked type I and type II collagenous matrices for the repair of full-thickness articular cartilage defects–a study in rabbits. Biomaterials 2003;24:3255–3263.

66 van Susante JL, Buma P, van Osch GJ et al. Culture of chondrocytes in alginate and collagen carrier gels. Acta Orthop Scand 1995;66:549–556.

67 Park YJ, Lee YM, Lee JY et al. Controlled release of platelet-derived growth factor-BB from chondroitin sulfate-chitosan sponge for guided bone regeneration. J Control Release 2000;67:385–394.

68 Camacho NP, West P, Torzilli PA et al. FTIR microscopic imaging of collagen and proteoglycan in bovine cartilage. Biopolymers 2001;62:1–8.

69 Huebsch N, Arany PR, Mao AS et al. Harnessing traction-mediated manipulation of the cell/matrix interface to control stem-cell fate. Nat Mater 2010;9:518–526.

70 Kato M, Mrksich M. Using model substrates to study the dependence of focal adhesion formation on the affinity of integrin-ligand complexes. Biochemistry 2004;43:2699–2707.

71 Robbins PD, Morelli AE. Regulation of immune responses by extracellular vesicles. Nat Rev Immunol 2014;14:195–208.

72 Murphy CM, Matsiko A, Haugh MG et al. Mesenchymal stem cell fate is regulated by the composition and mechanical properties of collagen-glycosaminoglycan scaffolds. J Mech Behav Biomed Mater 2012;11: 53–62.

73 Ignatius A, Blessing H, Liedert A et al. Tissue engineering of bone: effects of mechanical strain on osteoblastic cells in type I collagen matrices. Biomaterials 2005;26:311–318.

